Impedance Spectroscopy of Self-Assembled Monolayers on Au(111): Evidence for Complex Double-Layer Structure in Aqueous $NaClO_4$ at the Potential of Zero Charge

Richard P. Janek and W. Ronald Fawcett*

Department of Chemistry, University of California, Davis, California 95616

Abraham Ulman

Department of Chemistry, Brooklyn Polytechnic University, Brooklyn, New York 11202

Received: May 21, 1997; In Final Form: August 1, 1997[⊗]

The impedance of a Au(111) electrode modified by three different self-assembled monolayers has been studied over a wide frequency range in aqueous $NaClO_4$ solutions. The impedance characteristics of the bare electrode are compared with those of the same electrode modified with decanethiol, ω-hydroxydecanethiol, and 4′-hydroxy-4-mercaptobiphenyl. In the case of the decanethiol system the interfacial impedance can be represented as a capacitor due to the self-assembled monolayer in series with the solution resistance. However, for the latter two systems, the impedance behavior is more complex with a high resistance in the monolayer parallel to the expected capacitance. This behavior is quite different than that discussed to date in the literature and assumed in the interpretation of voltammetric data for modified electrodes. The parameters for these systems are reported here as a function of electrolyte concentration at the point of zero charge on the bare Au(111). The consequences of the present observations are discussed with respect to the phenomena observed for these systems.

Introduction

The accurate description of the electrical double layer is an essential component to understanding the nature of self-assembled monolayers (SAMs) as they are used in electrochemical systems. Most recent studies of the SAM double-layer structure have been performed in conjunction with electron-transfer measurements and have utilized, predominately, cyclic voltammetry as a means to observe the capacitance of the modified interface.[1−6] The interface has been considered as an ensemble of capacitors, connected in series with a solution resistance, which idealizes the behavior of the dielectric SAM coating and the classical diffuse layer capacity described by Gouy and Chapman.[8] In the present study this hypothesis was tested by examining the impedance spectra of SAMs on a Au(111) substrate as a function of electrolyte concentration and as a function of the nature of the SAM.

Long-chain alkanethiols are known to form monolayers on gold surfaces anchored by the gold−sulfur bond, interchain van der Waals forces, and headgroup interactions.[9] This structure is adjacent to the electrolyte solution and forms an idealized dielectric material. When the electrode is charged and electrostatic equilibrium is attained, the charge on the electrode is balanced by the charge in the solution. The charge separation can be described by two capacitors in series: the capacity of the SAM, C_{SAM}, and the electrolyte concentration-dependent capacity of the diffuse layer, C_{GC}, extending into the bulk of the electrolyte.

$$\frac{1}{C_{total}} = \frac{1}{C_{SAM}} + \frac{1}{C_{GC}} \tag{1}$$

C_{SAM} is understood to include any Stern layer consisting of hydrophobically bound water molecules between the actual SAM and the diffuse layer. When the interfacial capacity is measured, the total response will be dominated by the smaller term in the sum. In the case of SAMs there is at least an order of magnitude difference between C_{GC} ($\geqslant 20\ \mu F\ cm^{-2}$) and C_{SAM} ($\sim 2\ \mu F\ cm^{-2}$) depending on the electrolyte.

The interfacial capacity of a variety of SAMs, measured by dividing the observed cyclic voltammetric current by the scan rate in the absence of faradaic currents, has been reported.[1−6] The values are consistent with a simple dielectric model in which the SAM behaves ideally as a capacitor with a dielectric constant similar to bulk polyethylene and a capacitance that depends on the SAM thickness and the nature of the headgroup. Miller et al.[5] have probed the diffuse layer term of the interfacial capacity by observing the system as a function of electrolyte concentration and have estimated the potential of zero charge of alkanethiol and ω-hydroxythiol-coated Au electrodes.

Impedance spectroscopy[10] (IS) allows one to observe the magnitude of the interfacial capacity and the pattern of interconnectivity of the ideal circuit elements at a higher resolution than capacity measurements based on cyclic voltammetry or chronoamperometry. IS offers an excellent method to test the equivalent circuit model used to describe SAMs. A small-amplitude sinusoidal signal is applied to the electrochemical cell, and the current response is measured under potentiostatic control. The impedance

$$Z(j\omega) = \frac{\dot{V}(j\omega)}{\dot{I}(j\omega)} = Z'(\omega) + jZ''(\omega) \tag{2}$$

is calculated as the ratio of the system voltage phasor, $\dot{V}(j\omega)$, to the current phasor, $\dot{I}(j\omega)$, which are generated by a frequency response analyzer during the experiment. $Z(j\omega)$ is a complex quantity ($j = \sqrt{-1}$) and is a function of the excitation frequency, ω. Z' and Z'' can be calculated given an equivalent circuit model for the system using traditional algebraic methods of circuit analysis.[11] In the case of SAM modified electrodes it has been assumed that, for a series *RC* circuit,

$$Z'(\omega) = R_{solution} \tag{3}$$

and

[⊗] Abstract published in *Advance ACS Abstracts,* September 15, 1997.

S1089-5647(97)01698-2 CCC: $14.00

$$Z''(\omega) = -\frac{1}{\omega C_{\text{total}}} \quad (4)$$

It is shown here that this model is naive and cannot explain the impedance spectra of all SAM modified electrodes. In the present study the impedance of Au(111), Au(111) electrodes modified with decanethiol (DT), ω-hydroxydecanethiol (HDT), and 4′-hydroxy-4-mercaptobiphenyl (HMB) was measured in $NaClO_4$ solutions (see Figure 1) as a function of electrolyte concentration, and models for the electrochemical behavior of these systems are proposed. Parsons−Zobel plots[12] are used to separate the diffuse layer capacitance from the capacity of the SAM and extract values for C_{GC} and C_{SAM} for each system.

Experimental Section

Chemicals. Decanethiol (DT) was obtained from Aldrich and used as received. ω-Hydroxydecanethiol (HDT) was synthesized from 10-bromodecanol (Aldrich) by refluxing in 90% ethanol (Quantum Chemical)/water with 1.2 equiv of thiourea (Aldrich) for 5 h. The ethanol was removed by rotary evaporation. Then, 1.2 equiv of NaOH (Aldrich) in 20 mL of water was added to hydrolyze the thiouronium salt in situ followed by reflux for 30 min. The reaction mixture was extracted three times with chloroform (Aldrich). The crude product was separated on a silica gel (Baker) column with 5% ethyl acetate (Aldrich) in chloroform as the mobile phase with detection by TLC using iodine development; the large spot in the center of the plate was used. The final product was a slightly yellow viscous liquid at room temperature and gave a yield of 46%. Elemental analysis, H NMR, and ^{13}C NMR provided confirmation of structure. The elemental analysis results: expected (C, 63.01%; H, 11.65%; S, 16.84%); found (C, 62.95%; H, 11.71%; S, 15.21%).

4′-Hydroxy-4-mercaptobiphenyl (HMB) was prepared by palladium-assisted coupling of 4-(methylthio)phenylmagnesium bromide and 4-iodoanisol. Thus, the $Pd(PPh_3)_4$ catalyst (0.2 mmol, Aldrich) was added to 4.68 g (20 mmol) of 4-iodoanisol (Aldrich) in 5 mL of absolute THF (Aldrich), and the solution was brought to gentle reflux under dry nitrogen. A Grignard solution, prepared in the usual way from 1-bromo-4-methylthiobenzene (4.06 g, 20 mmol, Aldrich) and magnesium (22 mmol, Kodak) in 25 mL of THF, was transferred to the boiling 4-iodoanisol solution using a $^1/_8$ in. Teflon tubing. The entire system was under nitrogen, and nitrogen pressure was used to control the addition rate. The reaction was exothermic. First, the solution became clear, and then magnesium salts started to deposit. After the addition was completed, the mixture was refluxed for an additional 30 min. After cooling, the reaction mixture was poured into ice water (100 mL) containing 5 mL of HCl. The solid was filtered, washed with water, dried, and crystallized from heptane with some 2-propanol. The yield was 68%.

A 3.06 g (20 mmol) sample of 4-methoxy-4′-methylthiobiphenyl was dissolved in 30 mL of dry DMF (Aldrich) under a nitrogen blanket. C_2H_5SK (4.6 g, 50 mmol) was added to the stirred solution, and it was refluxed gently for 6 h. After cooling, the solution was poured into ice water (100 mL) containing 5 mL of HCl. The solid was collected, washed with cold water, air-dried, and crystallized from heptane/2-propanol. The yield of 4′-hydroxy-4-mercaptobiphenyl was 78%. The structure was confirmed by H NMR and ^{13}C NMR.

Sodium perchlorate (Fluka) was used as received. Nanopure water was obtained from a Barnstead filter system and had a resistivity of ∼18 MΩ cm.

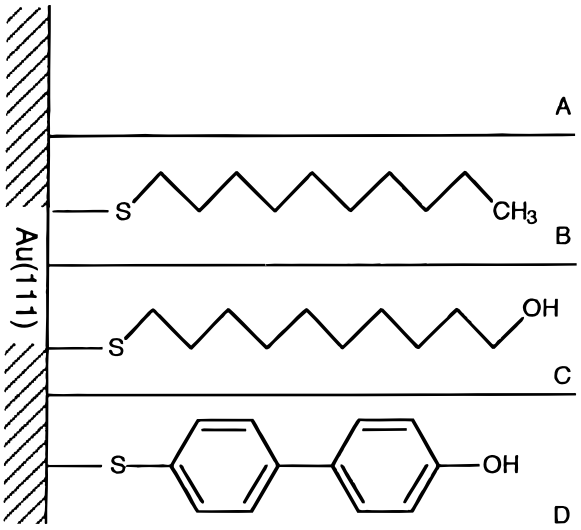

Figure 1. Schematic illustration of SAMs under consideration in this study showing (A) bare Au(111), (B) Au(111) modified with decanethiol (DT), (C) Au(111) modified with ω-hydroxydecanethiol (HDT), and (D) Au(111) modified with 4′-hydroxy-4-mercaptobiphenyl (HMB).

Electrochemical Cell and Instrumentation. A conventional three-electrode cell was used with a water jacket for temperature control and Teflon stopper with holes for electrode insertion and pure N_2 gas purge. All experiments were conducted at 25 ± 1 °C. The cell was enclosed in a grounded Faraday cage. A reference electrode was constructed by sealing a pure Ag wire into a glass tube with a solution of 0.01 M $AgClO_4$ and capped with a Vycor tip (stable after equilibration, −0.432 V vs SCE). The reference electrode was always isolated from the cell by a Luggin capillary containing the electrolyte. The $AgClO_4$ reference was used because $KClO_4$ has a limited solubility and would precipitate in the liquid junction of a saturated calomel electrode. The counter electrode was a large area pure gold leaf. Impedance was measured with a Solartron 1255 frequency response analyzer (FRA) interfaced to an EG&G 283 potentiostat/galvanostat. The current and voltage output signals from the potentiostat were fed into the channel 1 and channel 2 correlators of the FRA, and the impedance was reported as the ratio of the output of these analyzers. The data acquisition and control was handled by a Zenith 286 PC interfaced to the FRA and the potentiostat via the IEEE-488.2 general purpose interface bus (GPIB) and with software written in the C language in the DOS system. The instrument was thoroughly calibrated using the method of Sluyters et al.[13,14] by measuring the impedance of a collection of circuits composed of high-quality resistors and capacitors. Wave forms were monitored by an Iwatsu DS-6121 digital oscilloscope during data acquisition to ensure good signal quality. All glassware was cleaned by boiling in 50% HNO_3 for several hours and rinsed very well with Nanopure water (>17 MΩ cm^2) before each use.

Procedure. The single-crystal (111 face) gold working electrode was obtained from Metal Crystals and Oxides LTD, Cambridge, England. The electrode was prepared by polishing. The following procedure was used: hand polishing on silicon carbide P4000 grinding paper and then on a Buehler Ecomet 3 motorized wheel using wet alumina powder of finer and finer grades (from 3 μm down to 0.05 μm) on different felts according to Hamelin.[15] Once the surface of the electrode was observed to be defect-free under 30× magnification, the electrode was rinsed in water for 20 min and then cycled from −0.5 to 1.4 V vs SCE in 0.01 M $HClO_4$ at 50 mV s^{-1} until a stable baseline was obtained. The geometric area of the electrode was 0.0856

cm^2. The "true" area of the electrode was estimated by measuring the charge corresponding to the reduction of gold oxide after electrolysis at 1.5 V vs SCE for 100 s.[16] According to this procedure, a "roughness factor" of 1.65 was found for this electrode. All current densities and capacitances are reported here with respect to the *geometric* area. Electrode modification was conducted by dipping overnight in 30 mM ethanolic solutions of thiol at room temperature followed by rinsing in clean ethanol (5 min) and Nanopure water (5 min). The electrode was then transferred to the cell, using the hanging meniscus solution contact technique, for impedance measurements. After the experiment, the electrode was rinsed, placed in a Bunsen flame, and quenched in Nanopure water to remove the SAM. The Au(111) baseline in 0.01 M $HClO_4$ was obtained before modification and after it had been flame-treated to remove the SAM following the measurement. The electrode was stored in Nanopure water when not in use. The impedance measurements were performed at the potential of zero charge, with an applied bias voltage of 0.230 V vs SCE generated by the potentiostat, 5 mV rms sinusoidal excitation amplitude, and automatic analyzer integration time (0.001% SD of $\dot{I}(j\omega)$ correlator output) with a 100 s cutoff time. Measurements were made five times at each frequency and averaged during the run. The impedance was measured at 50 frequencies from 1 Hz to 100 kHz with 10 steps per decade. Each experiment was performed five times from modification to annealing, and the results were averaged. The impedance data were fit to an equivalent circuit model in the complex plane by using an algorithm based on that of Macdonald.[10] Both $-Z''$ and Z' data were used in the impedance fit (at the same time) using a complex nonlinear regression technique (CNLS) which included analytic first derivatives of the trial function and the Levenberg−Marquardt algorithm.[17] This program was written in C and run on a Macintosh PowerBook 145B computer.

Results

Cyclic Voltammetry. One of the advantages of working with single-crystal electrodes is that all experiments are performed on the same surface, which can be repeatedly cleaned and brought to the same initial conditions for each measurement. The cleanliness of the Au(111) surface is particularly evident by cyclic voltammetry in 0.01 M $HClO_4$. The gold metal interface in aqueous solutions has been observed thoroughly by Hamelin[18−20] and others.[21−22,37] However, there are few quantitative studies of the relationship between surface defects and cyclic voltammetry in 0.01 M $HClO_4$, in the sense that any defects are noticeable as distortions in the cyclic voltammogram, but it is often impossible to identify with certainty the etiology. The oxidation and reduction peaks are distorted, and the double-layer region is altered when the electrode is of poor quality. Figure 2 shows a cyclic voltammogram of Au(111) in 0.01 M $HClO_4$ displaying the oxidation and reduction of the gold surface and the electrolyte. This voltammogram is a superposition of 25 separate experiments and attests to the repeatability of this technique. The double-layer region of Au(111), that is, the potential range in which faradaic processes are absent, is shown in Figure 3 and is consistent with previously reported results.[37] In the absence of specific adsorption, the potential of zero charge (pzc) corresponding to the potential, ϕ, at which

$$dC_{GC}/d\phi = 0 \tag{5}$$

has the value of 0.21 ± 0.01 V vs SCE with a capacity of ~20 $\mu F\ cm^{-2}$ for Au(111) in 0.01 M $HClO_4$. This value for the pzc is slightly lower than most previously reported results, but it is within the standard deviation of the data given by Schmickler et al.[37] The lower pzc may indicate that the electrode used in this study has a small polycrystalline contribution. However, the voltammetry shown in Figure 2 does not support this. $NaClO_4$ was chosen as the electrolyte because of concern that $HClO_4$ at low pH might complicate the data interpretation due to its acidity. A more complex double layer would result if the hydroxyl headgroups of HDT and HMB were protonated in an environment of high proton activity. Therefore, the Au(111) baseline was determined in $NaClO_4$ and is shown in Figures 2 and 3. The pzc of Au(111) in 0.01 M $NaClO_4$, 0.23 ± 0.01 V vs SCE, is similar to the pzc in $HClO_4$. However, the oxidation and reduction peaks at the limit of the polarization range are broadened in $NaClO_4$.

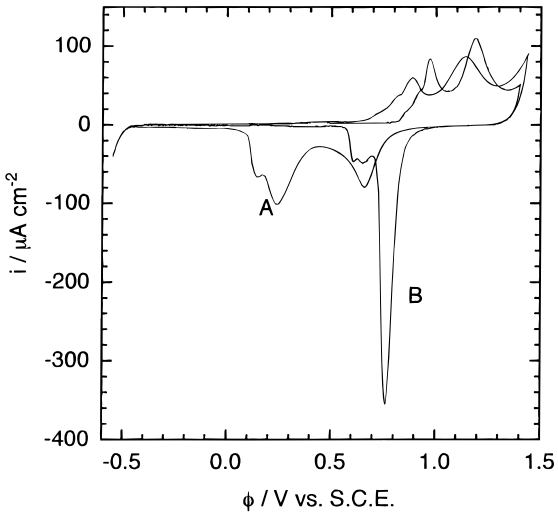

Figure 2. Cyclic voltammetry of Au(111) in (A) 0.01 M $NaClO_4$ and (B) 0.01 M $HClO_4$ at 50 mV s^{-1} from −0.5 V vs SCE to 1.45 V vs SCE. Initial potential, −0.5; sweep direction, positive.

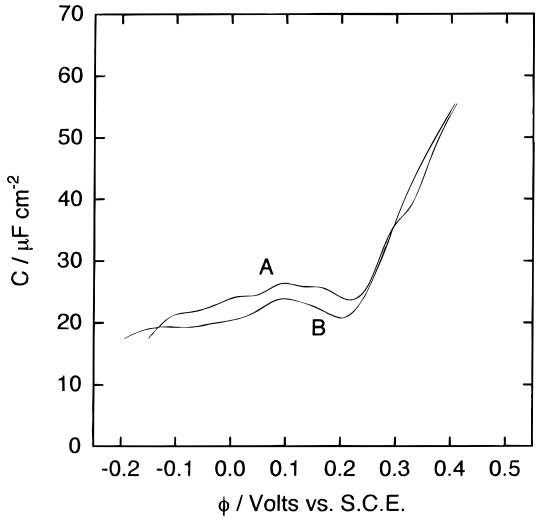

Figure 3. Differential capacitance of Au(111) measured in (A) 0.01 M $NaClO_4$ and (B) 0.01 M $HClO_4$ calculated from cyclic voltammetric data at 500 mV s^{-1}. The potential of zero charge, pzc, is visible as the minimum of the capacity curve at 230 mV vs SCE.

The Gouy−Chapman theory describes the capacity of the diffuse layer in the absence of specific adsorption as

$$C_{GC} = \frac{FA}{RT}\left(1 + \frac{\sigma_M}{4A^2}^2\right)^{1/2} \tag{6}$$

A is equal to $(2RT\epsilon_0\epsilon_s c_s)^{1/2}$; ϵ_s is the static dielectric constant of the pure solvent used in the experiments, ϵ_0 is the permittivity

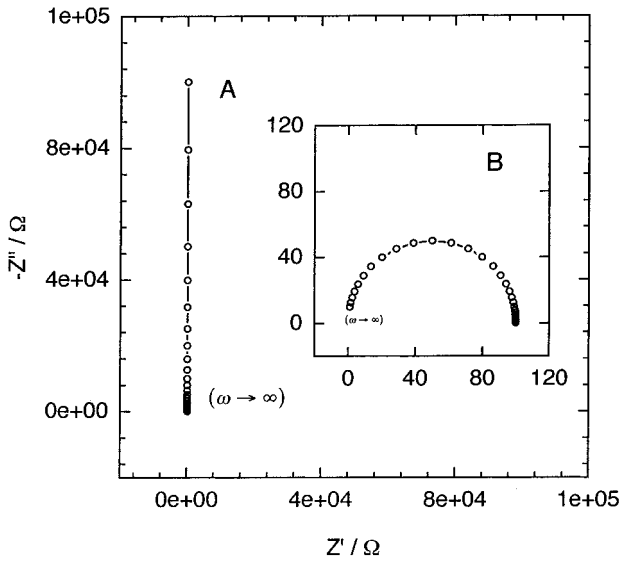

Figure 4. Theoretical Argand diagram plots for (A) a series combination of $R = 100\ \Omega$ and $C = 1.0 \times 10^{-6}$ F based on eqs 3 and 4 and (B) a parallel combination of the same values for R and C based on eqs 8 and 9. The frequency range was 10−100 000 rad s^{-1} at 10 steps per decade.

of free space, R and T have their usual meanings, c_s is the electrolyte concentration, and σ_M is the charge density on the electrode. In the absence of a SAM and ionic adsorption the observed capacity is dominated by that of the Stern layer, which consists of water molecules adsorbed on the metal electrode. In this case, eq 1 is written as

$$\frac{1}{C_{total}} = \frac{1}{C_S} + \frac{1}{C_{GC}} \tag{7}$$

where C_S is the capacity of the Stern layer. $1/C_{GC}$ dominates this sum when the electrolyte concentration is low and the electrode potential is near the pzc. When a SAM is present, one might consider writing eq 1 as the sum of three terms: one for the SAM, one for the Stern layer, and the third for the diffuse layer. However, there is no easy way to separate the first two terms. Because the capacity of the SAM is small compared to that of the diffuse layer over most of the potential range, the cyclic voltammogram is quite featureless at reasonable electrolyte concentrations; that is to say, the cyclic voltammogram of a SAM modified electrode looks like a straight line in the double-layer region.

Impedance Spectroscopy. The impedance of three SAM modified Au(111) electrodes was measured and compared to the case of bare Au(111). Systems with quite different properties were chosen, including decanethiol (DT) which has been studied extensively,[1,9] ω-hydroxydecanethiol (HDT),[2,3] and 4′-hydroxy-4-mercaptobiphenyl (HMB)[4,7] to compare a conjugated biphenyl system with an alkanethiol. One may suppose that a SAM formed with a biphenylthiol will behave differently than a SAM formed with an alkanethiol of equal length. It is known[9] that alkanethiol SAMs exhibit significant structural fluidity due to the mobility of the methylene carbons and may indeed form more compact monolayers due to these extra degrees of freedom. On the other hand, a biphenyl system is structurally rigid and lacks the internal rotations present in the alkanethiol molecule. The biphenyl SAM may be more loosely packed than the alkanethiol SAM and therefore permit ion permeation which can be observed with impedance spectroscopy.

There are several methods used to analyze impedance data. The data here are presented in the complex plane, a plot of $-Z''$ vs Z', or Argand space, with $-Z''$ so that the data appear in the first quadrant of the Cartesian plane. $-Z''$ and Z' are parametric functions of ω. The aim of this work is to generate an equivalent circuit, based upon an intuitive understanding of the physical situation at hand. From the equivalent circuit model it is possible to write down algebraic equations for $-Z''$ and Z' and fit the experimental data, in the complex plane, to obtain the magnitude of the ideal circuit elements. Finally, the ideal circuit elements are related to microscopic chemical processes occurring during the experiment.

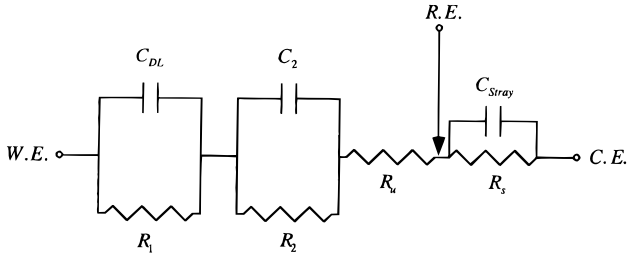

Figure 5. The general equivalent circuit model used to obtain equations for Z' and $-Z''$. The complex nonlinear regression results are shown in Table 1. W.E. is the working electrode, R.E. the SCE reference electrode, and C.E. the gold leaf counter electrode.

It is helpful to describe several features of impedance spectra in the complex plane in terms of the arrangement of circuit elements and the resulting structure of the spectra. This study involves the use of two patterns of connectivity of ideal resistors and capacitors. First, a series combination of R and C results in eq 1 and eq 2 for Z' and $-Z''$, respectively, and the Argand diagram for this circuit is shown in Figure 4 A. This is a typical model for the electrochemical interface in the absence of faradaic processes, and the complex plane representation is a vertical line with a high-frequency intercept at R. Second, a parallel combination of R and C is considered which results in a semicircle in the complex plane with

$$Z'(\omega) = \frac{R}{1 + (\omega RC)^2} \tag{8}$$

and

$$Z''(\omega) = \frac{-R^2C\omega}{1 + (\omega RC)^2} \tag{9}$$

The semicircle has a maximum in $-Z''$ at

$$\omega_p = 1/RC \tag{10}$$

with data points corresponding to the lowest frequencies near the origin (see Figure 4, plot B).

Figure 5 shows a general circuit that is capable of describing the impedance data observed experimentally. The values of the individual circuit elements are summarized in Table 1 and were obtained using the CNLS program described earlier. It must be emphasized that in many situations the equivalent circuit is much simpler and can be represented by capacitors C_{DL} and C_{stray} and the solution resistance R_S along with any uncompensated resistance R_U. The latter normally arises in an electrochemical experiment due to the fact that the reference electrode must be placed a finite distance from the working electrode and becomes more important as the electrolyte concentration decreases. C_{stray} represents stray capacitances of the leads and other features of the experimental setup. It is seen in the experimental data only at low concentrations. The large resistance R_1 in parallel to the interfacial capacity was apparent

TABLE 1: CNLS Regression Results[a]

	$C_{DL}/\mu F\ cm^{-1}$	$R_S/\Omega\ cm^2$	$R_U/\Omega\ cm^2$	$C_{stray}/\mu F\ cm^{-2}$	$R_1/\Omega\ cm^2$	$C_2/\mu F\ cm^{-2}$	$R_2/\Omega\ cm^2$
Au(111)							
1 M	22.9(1.2)	2.9(0.5)					
0.1 M	22.2(0.7)	27(8.1)					
0.01 M	20.6(0.7)	241(69)	11.4(1.7)	0.029(0.005)			
0.001 M	16.9(0.3)	2076(581)	98.3(10.3)	0.031(0.01)			
0.0001 M	13.2(0.8)	20240(4210)	1218(25.1)	0.029(0.004)			
DT							
1 M	1.73(0.08)	2.7(0.71)					
0.1 M	1.63(0.12)	20(9.1)					
0.01 M	1.61(0.09)	167(71)	13.7(0.9)	0.042(0.01)			
0.001 M	1.42(0.13)	1319(621)	139(11.7)	0.043(0.008)			
0.0001 M	1.25(0.21)	10280(5102)	673(97)	0.057(0.01)			
HDT							
1 M	3.65(0.31)	3.5(1.1)			31160(14130)		
0.1 M	2.89(0.07)	29(2.1)			310000(74400)		
0.01 M	2.54(0.19)	221(31)	14(5)	0.029(0.013)	167637(60120)		
0.001 M	2.40(0.91)	2131(65)	75(31)	0.027(0.008)	419100(60310)		
0.0001 M	2.16(0.65)	11130(4840)	971(219)	0.008(0.010)	499651(71940)		
HMB							
1 M	7.80(0.20)	3.5(0.6)			135(13)	65.1(2.9)	15000(4310)
0.1 M	6.04(0.14)	28(15)			1053(139)	61.3(7.8)	9931(231)
0.01 M	5.42(0.49)	206(61.8)	9.5(2.1)	0.028(0.01)	15130(2510)		
0.001 M	4.39(0.13)	1777(352)	131(13.9)	0.031(0.0075)	106200(21300)		
0.0001 M	3.83(0.91)	18740(3751)	951(52)	0.025(0.01)	255300(13401)		

[a] Standard deviation shown next to value. [b] See Figure 6 for equivalent circuit model.

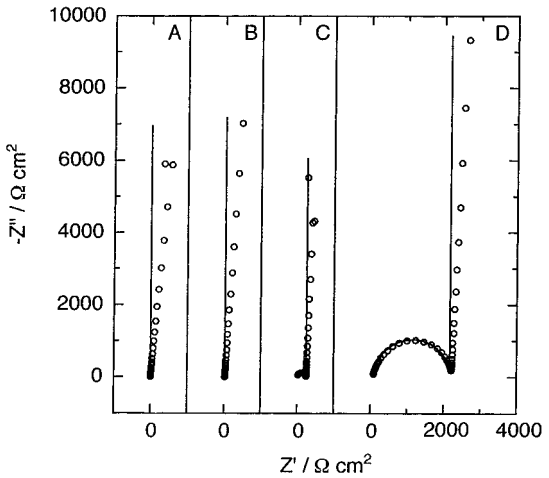

Figure 6. Argand space plots of the impedance of Au(111) in (A) 1 M $NaClO_4$ solution, (B) 10^{-1} M $NaClO_4$, (C) 10^{-2} M $NaClO_4$, and (D) 10^{-3} M $NaClO_4$; (○) experimental data, (—) fit to equivalent circuit model in Table 1. The plot for 10^{-4} M $NaClO_4$ is not shown but is similar to (D). The frequency range was 10 Hz to 100 kHz, and the applied bias potential was 230 mV against the SCE.

with two of the SAM systems as described below. One system had an extra parallel combination.

Figure 6 shows the impedance of Au(111) in aqueous $NaClO_4$ at four different electrolyte concentrations. The most noticeable feature of these data is the vertical line corresponding to the series combination of the interfacial capacity and the solution resistance. As the solution resistance increases to over 200 Ω cm^2, a small semicircle is observed at high frequencies as shown in plots C and D of Figure 6. The deviation or tilt of the data toward higher than expected values of Z' from the predicted response is the result of nonidealities of the solid Au(111) interface and has been discussed at length by several authors.[10,23−26] This geometry-induced artifact which is not observed at liquid Hg electrodes can be modeled as a power law-dependent interfacial capacity or constant phase element. This was not done in this study for two reasons: first, the correction is small (the exponent is very close to 1), and second, a more complicated model does not offer greater resolution of the interfacial properties of SAMs. It can be seen from the magnitude of the circuit elements obtained from CNLS fits to the data (Table 1) that C_{DL} corresponds to the interfacial capacity and has a concentration-dependent value from 22.9 to 13.2 $\mu F\ cm^{-2}$; R_s corresponds to the solution resistance. The high-frequency semicircle is observed at high solution resistance because the current flowing between the working and counter electrodes finds alternate pathways through stray capacitances, which are in parallel with the solution resistance of the system and present a lower impedance compared to the solution resistance.[27] This stray capacity is approximately 32 ± 12 nF and is present in all impedance spectra in the same frequency range. R_U increases from 11 Ω cm^2 at 10^{-2} M to 1220 Ω cm^2 at 10^{-4} M. At higher electrolyte concentrations it is not observed experimentally.

The Au(111) surface modified with decanethiol (DT) has an impedance spectrum similar to that of bare Au(111) in that one observes an interfacial capacity in series with a solution resistance at high electrolyte concentrations. The effects of stray capacitance and uncompensated resistance are also observed at lower electrolyte concentrations (Figure 7). The imaginary part of the impedance, $-Z''$, is approximately an order of magnitude greater than the $-Z''$ values for bare Au(111). This is due to the lower capacity of the Au(111)/SAM interface compared to the capacity of the Au(111) /$NaClO_4$ interface. Table 1 shows the results of the complex plane regression with interpretations analogous to the bare Au(111) system. The interfacial capacity for decanethiol SAM modified interfaces ranges from 1.73 to 1.25 $\mu F\ cm^{-2}$ as the electrolyte concentration ranges from 1 to 10^{-4} M. The data for decanethiol modified Au(111) show less deviation from 90° than do the bare Au(111) values, indicating that the CPE character of the impedance is somewhat less important in the presence of a decanethiol SAM.

The plots of Figure 8 show the impedance spectrum of Au-(111) modified by adsorption of ω-hydroxydecanethiol (HDT) in five electrolyte concentrations. These results are noticeably different from the previous data for bare Au(111) and DT modified Au(111). In the case of HDT a semicircle is seen at high concentrations rather than the capacitive behavior found for gold modified by DT. The radius of this semicircle increases

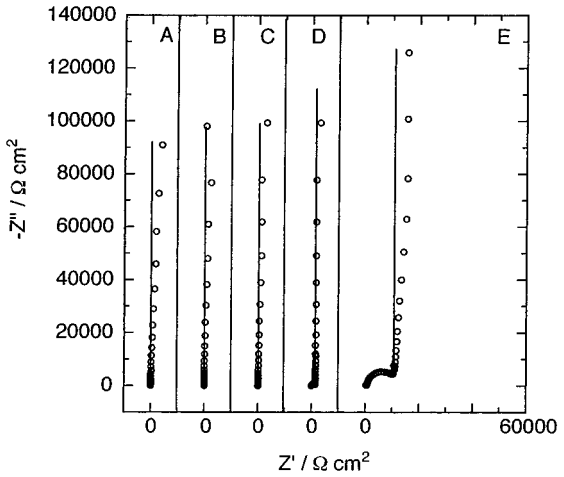

Figure 7. Argand space plots of the impedance of Au(111) modified with decanethiol (DT) in (A) 1 M $NaClO_4$ solution, (B) 10^{-1} M $NaClO_4$, (C) 10^{-2} M $NaClO_4$, (D) 10^{-3} M $NaClO_4$, and (E) 10^{-4} M $NaClO_4$; (○) experimental data, (—) fit to equivalent circuit model in Table 1 using CNLS. The frequency range was 10 Hz to 100 kHz, and the applied bias potential was 230 mV against the SCE.

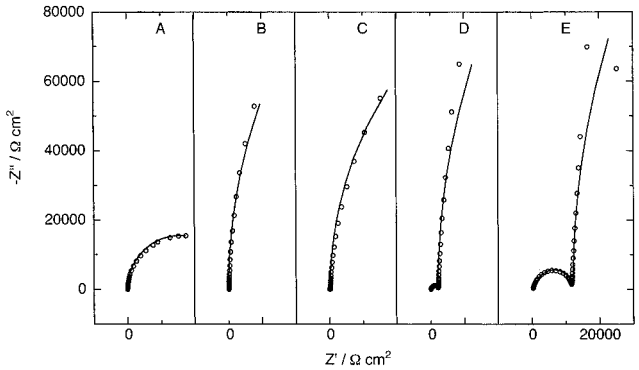

Figure 8. Argand space plots of the impedance of Au(111) modified with ω-hydroxydecanethiol (HDT) in (A) 1 M $NaClO_4$ solution, (B) 10^{-1} M $NaClO_4$, (C) 10^{-2} M $NaClO_4$, (D) 10^{-3} M $NaClO_4$, and (E) 10^{-4} M $NaClO_4$; (○) experimental data, (—) fit to equivalent circuit model in Table 1 using CNLS. The frequency range was 10 Hz to 100 kHz, and the applied bias potential was 230 mV against the SCE.

with decreasing electrolyte concentration and indicates that a large resistance is in parallel with the double-layer capacity. The latter parameter, C_{DL}, ranges from 3.65 μF cm^{-2} at 1 M to 2.16 μF cm^{-2} at 10^{-4} M $NaClO_4$. The solution resistance and stray capacity are similar to the previous systems. The unexpected parallel interfacial resistance increases approximately linearly from 30 000 to 500 000 Ω cm^2 with decrease in the electrolyte concentration.

Figure 9 shows the impedance spectrum for 4′-hydroxy-4-mercaptobiphenyl (HMB) modified Au(111) and bears a close resemblance to the HDT system. However, there are some noticeable differences. For each concentration of $NaClO_4$ *two* parallel *RC* circuit elements are observed as two merged semicircles in the Argand diagram. The impedance spectrum in 1 M $NaClO_4$ shows unexpected behavior. Plot A of Figure 9 shows that there are two parallel *RC* elements: one with a capacity of 7.80 μF cm^{-2} in parallel with 135 Ω cm^2 and the second with a capacity of 65.1 μF cm^{-2} in parallel with 15 000 Ω cm^2. These are followed by a solution resistance of 3.5 Ω cm^2, which is the expected result at this concentration. Following a 10-fold dilution of the supporting electrolyte, another pair of parallel *RC* combined circuit elements with a capacity of 6.04 μF cm^{-2} in parallel with 1053 Ω cm^2 and a capacity of 61.3 μF cm^{-2} in parallel with 9931 Ω cm^2 followed by a

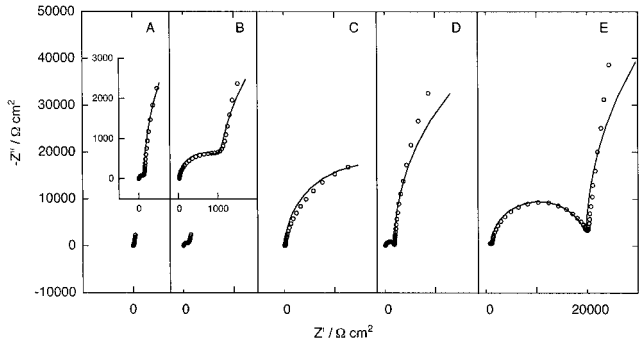

Figure 9. Argand space plots of the impedance of Au(111) modified with 4′-hydroxy-4-mercaptobiphenyl (HMB) in (A) 1 M $NaClO_4$ solution, (B) 10^{-1} M $NaClO_4$, (C) 10^{-2} M $NaClO_4$, (D) 10^{-3} M $NaClO_4$, and (E) 10^{-4} M $NaClO_4$; (○) experimental data, (—) fit to equivalent circuit model Table 1 using CNLS. (A) and (B) have been expanded to show the details at high electrolyte concentration. The frequency range was 10 Hz to 100 kHz, and the applied bias potential was 230 mV against SCE.

solution resistance of 27.8 Ω cm^2 are found in plot B. The first resistance, R_1, increases by approximately an order of magnitude, while the other values remain approximately constant. As the electrolyte concentration is decreased further (see plot C), one of the parallel *RC* semicircles vanishes and is replaced by the combination of the stray capacity and the solution resistance. At 0.01 M $NaClO_4$ and beyond the large capacity is no longer observed, but a capacity of 5.42 μF cm^{-2} is found in parallel with an interfacial resistance of 15 000 Ω cm^2.

Discussion

IS can be an ideal technique to examine a system in which the *conductivity* is influenced by specific microscopic events of interest. The excitation frequencies are usually between 1 mHz and 1 MHz; therefore, relaxation times over 9 decades from minutes to microseconds are probed. The choice of frequency range depends on what relaxation process is considered. The middle frequency of the range should correspond to ω_p (eq 10). One of the processes occurring in electrochemical systems is the relaxation of the electrical double layer, and for typical values of R and C this occurs on the order of 60 μs. The conduction path of the interfacial system is the charging and discharging of the Au(111) electrode in the surrounding medium, and generally the linear combination of capacitors model is used to explain the response of the system to electrical stimulation; interpretation of the impedance follows accordingly.

There are two approaches used to understand impedance data. One can reconcile the data within the context of microscopic equations of motion, driven by an harmonic voltage excitation, or use an equivalent circuit model based upon the appearance of the impedance spectrum and a physical model of the system. Both methods have their advantages and disadvantages. The ab initio calculation of the current response involves the use of detailed microscopic models but may be too complicated to solve for the current response. The equivalent circuit method uses relatively simple algebraic equations to obtain values of the idealized circuit elements which are then related to underlying microscopic phenomena. The bane of the equivalent circuit method is that one is not assured of the uniqueness of the circuit model. However, this should not preclude its effective use in elucidating the physics and chemistry of conducting systems. It is possible to perform experiments as a function of several independent variables and observe the impedance as the system is varied. Often, one or more ideal circuit elements will

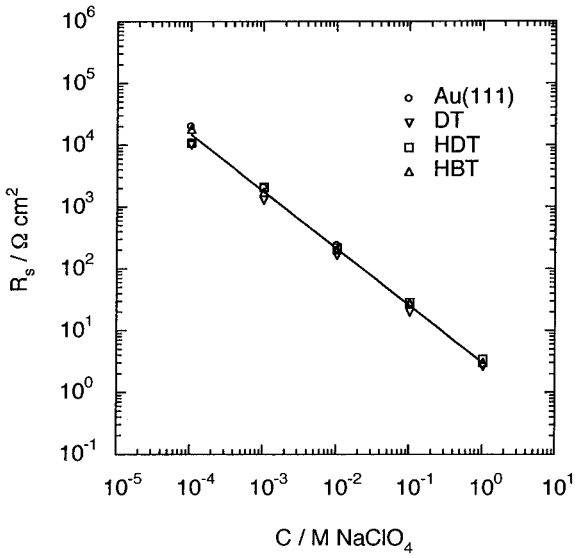

Figure 10. A plot of the solution resistance against electrolyte concentration showing the linear dependence of R_s on electrolyte concentration. The solid line is a linear regression through the average values.

correlate with the independent variable in a logical fashion which can be understood.

The elements of the circuit model are assigned to microscopic processes. In each experiment the electrolyte concentration was varied from 1 to 10^{-4} M, and it is expected that the circuit element associated with the solution resistance will decrease linearly over 5 orders of magnitude. Figure 10 shows a plot of the solution resistance as a function of electrolyte concentration. The values were obtained from the respective equivalent circuit model in Figure 5 and regression data in Table 1. The percent error of the solution resistance was between 25% and 30% due to variations in electrode placement in the cell. Also, at low electrolyte concentrations a linear dependence of the uncompensated solution resistance from approximately 10 to 1000 Ω cm^2 was observed. The uncompensated resistance is present at higher electrolyte concentrations, but it is vanishingly small and therefore unobserved in series with the solution resistance at low electrolyte concentrations. The linear variation of the solution resistance and the uncompensated resistance due to ionic motion is directly proportional to the electrolyte concentration.

The contributions from the interfacial capacity to the equivalent circuit capacity were analyzed as a function of the nature of the SAM. It is clear that there are only two types of capacitors for bare Au(111) and Au(111) modified by decanethiol: an interfacial capacity and a stray capacity. The interfacial capacity varies with the concentration and is an order of magnitude smaller for decanethiol. The values agree quite well with previously reported[1] data for these systems. Therefore, the interpretation is relatively straightforward in these two cases. However, Au(111) modified by ω-hydroxydecanethiol is unique in the sense that there is an unexplained parallel resistance along with the interfacial capacity. The interfacial capacity is in agreement with previously measured values by Miller et al.[2]

The magnitude of the parallel resistance for the HDT system is between 30 000 Ω cm^2 at 1.0 M $NaClO_4$ and 500 000 Ω cm^2 at 10^{-4} M $NaClO_4$ and is approximately linear in concentration within the error of the measurement. The resistance does not change with potential over the potential range −0.3 to 0.3 V vs SCE. This parallel resistance is assumed to be nonfaradaic in origin but must be associated with some conduction process. The supposition of the nonfaradaic origin of the resistance is probably sound, considering that all experiments were performed at potentials far from the formal potential of any redox species present. At this point, until further in situ experiments can be performed, it is hypothesized that the nature of the parallel resistance is related to some type of pore structure in the SAM, resulting in ion or solvent permeation or rearrangement of thiolate dipoles in the double layer. This type of interpretation is used often in IS studies of corrosion-inhibiting coatings.[27−30] There have been few studies investigating the permeability of SAMs, but polarization modulation infrared reflection absorption spectroscopy (PM-IRRAS) measurements of decanethiol monolayers indicate that the solvent interacts weakly with the SAM.[31] However, one cannot extrapolate this study to hydroxyl-terminated monolayers in solution which show this anomalous behavior. The observation of a parallel resistance does not mean that ω-hydroxydecanethiol SAMs are ineffective barriers to charge transfer as this would be in contradiction to reported electron-transfer studies involving this system.[2,3]

The situation for 4′-hydroxy-4-mercaptobiphenyl is more complex than ω-hydroxydecanethiol. A similar parallel combination of C and R which one may attribute to the interfacial capacity and a parallel resistance is observed. These resisitances are also independent of potential over the potential range −0.3 to 0.3 V vs SCE. However, there are now two types of interfacial capacities and two types of parallel resistances for HMB in 1 M $NaClO_4$ and 0.1 M $NaClO_4$. One of the two parallel combinations of R and C is only present for HBT in 1 and 0.1 M electrolyte solutions. This suggests that any structural domains responsible for the effect may be concentration dependent. The surface concentrations and the existence of different absorbate binding sites have been probed by the reductive desorption technique of Porter.[32] Unfortunately, the reductive desorption peak observed in these experiments is most likely complicated by disproportionation of the HMB at the surface of the electrode. This mechanism is currently under investigation in our laboratory. Again, until in situ spectroscopic measurements can be performed, the exact nature of the interfacial resistances and capacitances cannot be resolved completely. At this point it is concluded that ω-hydroxybiphenylthiol modified Au(111) electrodes display a complex double-layer structure with at least two regions of different interfacial capacities and parallel resistances which probably are related to different structural domains within the SAM. One may even question whether a compact monolayer, in contrast to a multilayer, is formed at all in this system. The characteristic relaxation times of these systems are on the order of seconds to minutes if one considers the product of R and C. For example, the relaxation times for HDT modified Au(111) are 0.11, 0.90, 0.43, 1.00, and 1.08 s, while the relaxation times for HMB are 0.12, 0.06, 0.82, 0.47, and 0.98 s. These values are quite large when compared to the 70 μs required to charge and discharge the aqueous gold interface.

Since the interfacial capacitance was measured as a function of concentration for these systems (see Figure 11), it is possible to examine the model based on a linear combination of capacitors (eq 1) in some detail using the Parsons−Zobel[12] plot. A plot of the inverse of the total interfacial capacity against the inverse of the calculated Gouy−Chapman capacity (eq 6) for different electrolyte concentrations is shown in Figure 12 and gives an estimate of the inner layer capacity. If we assume that the charge density on the electrode is constant and equal to zero at each concentration, the intercept of the Parsons−Zobel plot gives a value for the capacity of the SAM separate

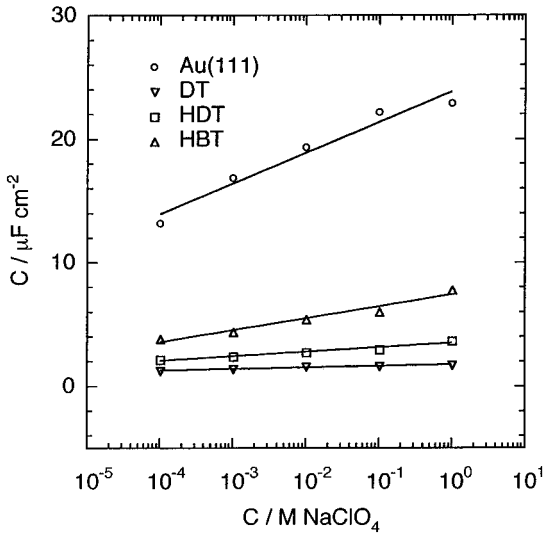

Figure 11. Plot of the total interfacial capacitance against electrolyte concentration. The solid line is the linear regression.

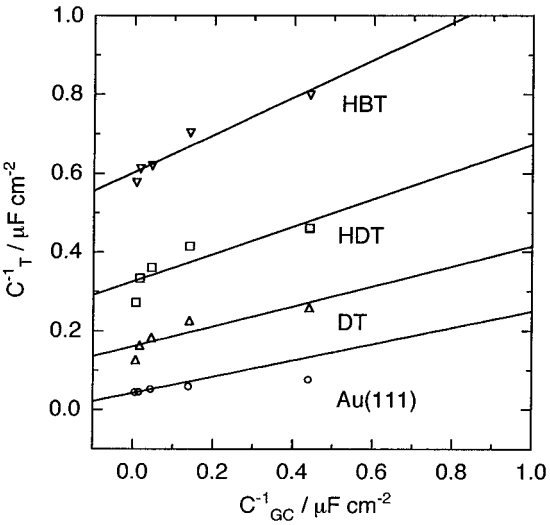

Figure 12. Parsons−Zobel plots of the four systems at the pzc. The solid line drawn through the data is the weighted linear least-squares regression.

TABLE 2: Parsons−Zobel Linear Regression Results[a]

	Au(111)	DT	HDT	HBT
intercept	0.0425(0.005)	0.603(0.015)	0.326(0.024)	0.161(0.016)
slope	0.210(0.01)	0.476(0.073)	0.348(0.120)	0.254(0.078)
C_S/μF cm^{-2}	23.5(0.92)	1.66(0.04)	3.07(0.22)	6.21(0.62)
1/slope	4.76(0.23)	2.10(0.32)	2.87(0.34)	3.94(0.31)

[a] Standard deviation shown next to value.

from the capacity of the diffuse layer. The inner layer, or SAM, capacity for decanethiol is 1.66 , 3.07 μF cm^{-2} for HDT and 5.31 μF cm^{-2} for HMB (see Table 2). The Parsons−Zobel plots shown in this work have slopes that are not equal to unity. It is known that unit slopes are observed when the electrode is liquid mercury in nonspecifically adsorbing electrolytes.[12] However, for solid electrodes Parsons−Zobel plots have slopes lower than unity due to the fact that the electrode is not perfectly smooth.[33−37] In addition, Borkowska and Jarzabek[38] have shown that the slopes of these plots are concentration-dependent at polycrystalline Au electrodes. This may account for the curvature seen in the data presented in Figure 12. If one ignores the concentration dependence and estimates the roughness on the basis of the linear fit, the values obtained here range from 2.1 to 4.8. The complicating features discussed by Borkowska and Jarzabek[38] show that this is not a definitive way of determing the actual roughness of the electrode. Thermally deposited Au(111)/mica electrodes with presumably lower "roughness factors" may provide an interesting comparison to bulk single-crystal Au electrodes used in this study.

The intercept of the Parsons−Zobel plot for bare Au(111), 23.5 μF cm^{-2} in $NaClO_4$, is consistent with Au(111) in the absence of a specifically adsorbing electrolyte.[31] The SAM capacity for decanethiol, 1.66 μF cm^{-2}, is similar to reported values ($\sim$1.65 μF cm^{-2}).[1] However, the inner layer capacity value for HDT is 69% higher than the capacity reported by Miller (2.11 μF cm^{-2}) in 0.1 M KCl. SAMs formed from 4′-hydroxy-4-mercaptobiphenyl have received no previous attention. However, Sabatani et al.[4] have measured the faradaic impedance of Au(111) in 0.5 M KCl modified by *p*-biphenyl mercaptan and report an interfacial capacitance of 4.5 μF cm^{-2}. The differences in the inner layer capacities are due to varying bulk dielectric constants of the molecules comprising the individual SAMs.

Conclusions

The impedance spectrum of Au(111) and Au(111) modified with decanethiol, ω-hydroxydecanethiol, and 4′-hydroxy-4-mercaptobiphenyl can be measured in $NaClO_4$ solutions over a wide concentration range. IS provides a sensitive means to examine the assumed ideal circuit model for interfacial systems and may be used to resolve the current−voltage relationships typically observed by cyclic voltammetry. This study has shown that a simple model of a series capacitor and resistor is naive and not sufficient to accurately fit the data of all SAM modified electrodes. The useful frequency range for the impedance measurement is from 1 Hz to 10 kHz depending on the solution resistance. At higher frequencies the stray capacitance of the system makes a larger contribution to the impedance. The presence of stray capacitances is observed when the solution resistance is greater than 200 Ω cm^{-2}. Simple equivalent circuit models are adequate to describe the impedance data for these systems. Assignment of the ideal circuit elements to microscopic chemical and physical processes can be made.

This study is interesting in the sense that a simple series combination of an interfacial capacitance and solution resistance cannot account for all SAM impedance spectra. If one is to use a SAM modified electrode as an analytical device to study fast electron transfer reactions or to investigate the properties of SAMs in their own right, the complex nature of the double layer must be considered. Often the application of cyclic voltammetry or potential step chronoamperometry to SAM modified electrodes assumes the simplest model for the charging of the double layer: this study proves that a naive model cannot be used for all systems. The SAM modified interface may take 4 orders of magnitude longer to relax than a bare metal aqueous interface. This longer relaxation time will severely affect the analysis of chronoamperometric data which often assumes a rapid double-layer charging. There appears to be a parallel conduction pathway to the charge flowing into the capacity of SAMs formed by ω-hydroxydecanethiol and 4′-hydroxy-4-mercaptobiphenyl on Au(111), both systems with hydroxy-terminated molecules. This conduction pathway might be due to ion permeation into the bulk of the SAM or to reorientation of thiols in the interface. The relaxation time of these processes are on the order of seconds to minutes depending on the particular values of *R* and *C*. If these relaxation times are related to some slow molecular motion, it must be characterized by a significant activation barrier. A measurement of the temperature dependence of this resistive component might be able to

distinguish such a high activation energy motion from a more pathological source which is not activated like pores in the monolayer. This phenomenon is being investigated in this laboratory using subtractively normalized interfacial FTIR spectroscopy (SNIFTIRS) as a means to probe further the structure of the SAM and continuing electrochemical measurements.

Acknowledgment. We acknowledge the helpful comments of Professors Zofia Borkowska and Cary Miller. Financial support of the National Science Foundation through Grant CHE 94-11659 is also gratefully acknowledged.

References and Notes

(1) Chidsey, C. E. D.; Loiacono, D. N. *Langmuir* **1990**, *6*, 682−691.
(2) Miller, C. J.; Cuendet, P.; Gratzel, M. *J. Phys. Chem.* **1991**, *95*, 877−886.
(3) Miller, C. J.; Gratzel, M. *J. Phys. Chem.* **1991**, *95*, 5225−5233.
(4) Sabatani, E.; Cohen-Boulakia, J.; Bruening, M.; Rubinstein, I. *Langmuir* **1993**, *9*, 2974−2981.
(5) Becka, A. M.; Miller, C. J. *J. Phys. Chem.* **1993**, *97*, 6233−6239.
(6) Cheng, J.; Saghi-Szabo, G.; Tossell, J. A.; Miller, C. J. *J. Am. Chem. Soc.* **1996**, *118*, 680−684.
(7) Creager, S. E.; Steiger, C. *Langmuir* **1995**, *11*, 1852−1854.
(8) Delahay, P. *Double Layer and Electrode Kinetics*; Wiley-Interscience: New York, 1965; Chapter 3 and references therein.
(9) Ulman, A. *An Introduction to Ultrathin Organic Films*; Academic Press: New York, 1991, and references therein.
(10) *Impedance Spectroscopy: Emphasizing Solid Materials and Systems*; Macdonald, J. R., Ed.; John Wiley & Sons: New York, 1987.
(11) *Mathematical Techniques: An introduction for the engineering, physical, and mathematical sciences;* Jordan, D. W., Smith, P., Eds.; Oxford University Press: Oxford, 1994; p 323.
(12) Parsons, R.; Zobel, F. G. R. *J. Electroanal. Chem.* **1965**, *9*, 333−348.
(13) Bongenaar, C. P. M.; Sluyters-Rehbach, M.; Sluyters, J. H. *J. Electroanal. Chem.* **1980**, *109*, 23−39.
(14) Andreu, R.; Gonzalez-Arjona, D.; Dominguez, M.; Molero, M.; Roldan, E. *Electroanalysis* **1991**, *3*, 377−383.
(15) Hamelin, A. In *Modern Aspects of Electrochemistry*; Conway, B. E., White, R., Bockris, J. O'M., Eds.; Plenum Press: New York, 1985; No. 16, Chapter 1.
(16) Woods, R.; Rand, D. A. J. *J. Electroanal. Chem.* **1971**, *31*, 29−38.
(17) *Numerical Recipes in C*, 2nd ed.; Press, W. H., Teukolsky, S. A., Vetterling, W. T., Flannery, B. P., Eds.; Cambridge University Press: New York, 1992; p 656.
(18) Hamelin, A. *J. Electoanal. Chem.* **1986**, *210*, 303−309.
(19) Hamelin, A.; Vitanov, T.; Sevastyanov, E.; Popov, A. *J. Electroanal. Chem.* **1983**, *145*, 225−264.
(20) Hamelin, A.; Doubova, L.; Wagner, D.; Schirmer, H. *J. Electroanal. Chem.* **1987**, *220*, 155−160.
(21) Lecoeur, J.; Andro, J.; Parsons, R. *Surf. Sci.* **1982**, *114*, 320−330.
(22) Trasatti, S. *J. Electroanal. Chem.* **1992**, *329*, 237−246.
(23) Scheider, W. *J. Phys. Chem.* **1975**, *79*, 127.
(24) Brug, G. J.; Van Den Eden, A. L. G.; Sluyters-Rehbach, M.; Sluyters, J. H. *J. Electroanal. Chem.* **1984**, *176*, 275−295.
(25) Pajkossy, T. *J. Electroanal. Chem.* **1994**, *364*, 111.
(26) Fawcett, W. R.; Kovačova, Z.; Motheo, A. J.; Foss Jr., C. A. *J. Electroanal. Chem.* **1992**, *326*, 91.
(27) Stewart, K. C.; Kolman, D. G.; Taylor, S. R. In *Electrochemical Impedance: Analysis and Interpretation*; Scully, J. R., Silverman, D. C., Kendig, M. W., Eds.; ASTM: Philadelphia, 1993; pp 73−93.
(28) Armstrong, R. D.; Wright, J. D.; Handyside, T. M. *J. Appl. Electochem.* **1992**, *22*, 795−800.
(29) Mansfeld, F. *Electrochim. Acta* **1993**, *38*, 1891−1897.
(30) Bonora, P. L.; Deflorian, F.; Fedrizzi, L. *Electrochim. Acta* **1996**, *41*, 1073−1082.
(31) Anderson, M. R.; Evaniak, M. N.; Zhang, M. *Langmuir* **1996**, *12*, 2327−2331.
(32) Walczak, M. M.; Alves, C. A.; Lamp, B. D.; Porter, M. D. *J. Electroanal. Chem.* **1995**, *396*, 103−114.
(33) Hamelin, A.; Stoicoviciu, L. *J. Electroanal. Chem.* **1989**, *271*, 15−26.
(34) Valette, G. *J. Electroanal. Chem.* **1982**, *138*, 37−54.
(35) Valette, G. *J. Electroanal. Chem.* **1981**, *122*, 285−297.
(36) Parsons, R. *Chem. Rev. (Washington, D.C.)* **1990**, *90*, 813−826.
(37) Eberhardt, D.; Santos, E.; Schmickler, W. *J. Electroanal. Chem.* **1996**, *419*, 23−31.
(38) Borkowska, Z.; Jarzabek, G. *Electrochim. Acta* **1997**, *42*, 2915−2918.